

FRF Measurement of Nonlinear Systems Operating in Closed Loop

Rik Pintelon, *Fellow, IEEE*, and Johan Schoukens, *Fellow, IEEE*

Abstract—To prevent unstable behavior or saturation, a frequency response function (FRF) measurement is often performed under closed-loop conditions (e.g., open-loop gain measurements of an operational amplifier). The difficulty of such FRF measurements is that the nonlinear (NL) distortions also perturb the input via the feedback loop. The latter introduces a bias in the estimate of the best linear approximation (BLA) and jeopardizes the interpretation of the output NL distortions. In this paper, we solve these problems via a generalized definition of the BLA that is valid for NL systems operating in feedback. The classical definition for open-loop systems follows as a special case.

Index Terms—Best linear approximation (BLA), feedback, frequency response function (FRF), nonlinear (NL).

I. INTRODUCTION

FREQUENCY response function (FRF) measurements give a lot of insight in the dynamic behavior of a system. It is used for analysis, design, prototyping, and modeling in all kinds of engineering applications, even if it is known that the system is subject to nonlinear (NL) distortions. The major reason for this is that the linear theory is well understood and easy to apply. Moreover, the impact of NL distortions on FRF measurements has been studied in detail [1]–[7]. Via well-designed experiments, one can estimate the FRF [called the best linear approximation (BLA)], its noise variance, and the level of the NL distortions [6]–[11]. As such, the user can decide whether the linear approximation is accurate enough or not for the intended application. If not, then a full NL modeling is required.

Although the theory of the BLA of an NL system has been developed for the open-loop case only [1], [3], [12], it has been applied with success to closed-loop situations without formal proof [9]–[11], [13]. However, due to the feedback loop, the input of the NL system is also disturbed by the NL distortions. This leads to a biased estimate of the classical BLA defined for open-loop systems and complicates the interpretation of the NL distortions in the output spectrum. In [14], only the first

Manuscript received June 4, 2012; revised August 30, 2012; accepted September 1, 2012. Date of publication October 9, 2012; date of current version April 3, 2013. This work was supported in part by the Research Council of the Vrije Universiteit Brussel, by the Research Foundation Flanders (FWO-Vlaanderen), by the Flemish Government (Methusalem Fund METH1), and by the Belgian Federal Government (Interuniversity Attraction Poles program VII, Dynamical Systems, Control, and Optimization). The Associate Editor coordinating the review process for this paper was Dr. Dario Petri.

The authors are with the Department of Electrical Engineering, Vrije Universiteit Brussel, 1050 Brussel, Belgium (e-mail: Rik.Pintelon@vub.ac.be; johan.schoukens@vub.ac.be).

Digital Object Identifier 10.1109/TIM.2012.2220033

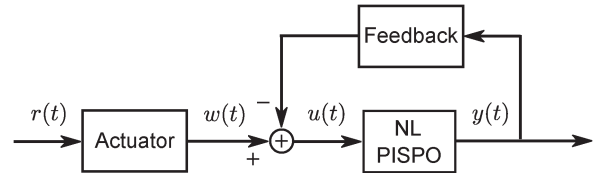


Fig. 1. NL PISPO system operating in a closed-loop configuration.

problem is handled assuming that the actuator and the feedback are linear. The aim of this paper is to solve both problems without imposing any linearity condition on the actuator and feedback dynamics.

First, inspired by the indirect FRF measurement method for linear feedback systems [15], [16], we propose a generalized definition of the BLA that is suitable for NL systems operating in closed loop. Moreover, the actuator and/or feedback dynamics might be NL. For open-loop systems driven by linear actuators, the generalized BLA reduces to the classical definition. Next, we prove that the existing methods for measuring the BLA [9], [10], [12] are still appropriate under feedback conditions. It explains why the feedback experiments in [9]–[11] and [13] were successful. Furthermore, we study the influence of the NL behavior of the actuator, prove that the linear feedback dynamics can be estimated from the open-loop gain measurements, and discuss the detection, classification, and quantification of the NL distortions in the presence of a feedback loop. Finally, the theory is illustrated on simulations and on open-loop gain measurements of an operational amplifier (opamp).

II. BLA OF AN NL SYSTEM

The class of NL systems considered includes the systems whose output can be approximated arbitrarily well in mean square sense by a Volterra series (see [1] and [17] for the details). This excludes phenomena such as chaos and bifurcations but allows for hard nonlinearities such as saturation, clipping, dead zones, etc. Since the steady-state response of such systems to a periodic input is periodic with the same period as the input, they will be denoted in the sequel of this paper as NL period in same period out (PISPO) systems.

The properties of the BLA of NL PISPO systems are studied for the class of Gaussian-like excitation signals. This class includes Gaussian noise, periodic Gaussian noise, and random phase multisines with the same Riemann equivalent power spectrum (see [7] for the details). First, we recall briefly the results for the open-loop case and next handle the closed-loop configuration (see Fig. 1).

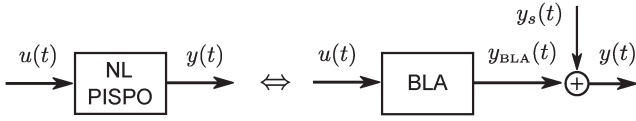


Fig. 2. BLA of an NL PISPO system.

A. Open-Loop Case

For NL PISPO systems operation in open loop (Fig. 1 without feedback branch), the BLA is defined as

$$G_{\text{BLA}}(j\omega) = \frac{S_{yu}(j\omega)}{S_{uu}(j\omega)} = \frac{F\{\mathbb{E}\{y(t)u(t-\tau)\}\}}{F\{\mathbb{E}\{u(t)u(t-\tau)\}\}} \quad (1)$$

with $S_{yu}(j\omega)$ being the input–output cross-power spectrum, $S_{uu}(j\omega)$ being the input autopower spectrum, and $F\{x(t)\}$ being the Fourier transform of $x(t)$, where the expected values $\mathbb{E}\{\cdot\}$ are taken w.r.t. the random excitation $u(t)$. The difference $y_s(t)$ between the actual output $y(t)$ of the NL system and the output $y_{\text{BLA}}(t)$ predicted by the BLA (1) (see Fig. 2) has some special properties.

For any class of random excitations with the same power spectrum and probability density function, we have the following:

- 1) $y_s(t)$ has zero mean: $\mathbb{E}\{y_s(t)\} = 0$.
- 2) $y_s(t)$ is uncorrelated with—but not independent of—the input $u(t)$: $\mathbb{E}\{y_s(t)u(t-\tau)\} = 0$.
- 3) $y_s(t)$ contains no subharmonics (harmonically related to the input $u(t)$).

where the expected values are taken w.r.t. the random input $u(t)$ (see [3], [4], and [18]).

For the class of Gaussian-like random excitations with the same power spectrum, the discrete Fourier transform (DFT) spectra $Y_S(k)$ and $U(k)$ of $y_s(t)$ and $u(t)$, respectively

$$X(k) = \frac{1}{\sqrt{N}} \sum_{t=0}^{N-1} x(t)e^{-j2\pi kt/N} \quad (2)$$

with $X = Y_S$, U and $x = y_s$, u having the following (additional) properties:

- 1) $Y_S(k)$ has zero mean: $\mathbb{E}\{Y_S(k)\} = 0$.
- 2) $Y_S(k)$ is uncorrelated with—but not independent of— $U(k)$: $\mathbb{E}\{Y_S(k)\bar{U}(k)\} = 0$.
- 3) $Y_S(k)$ contains no subharmonics (harmonically related to the input $U(k)$).
- 4) $Y_S(k)$ is asymptotically ($N \rightarrow \infty$) normally distributed.
- 5) $Y_S(k)$ is asymptotically ($N \rightarrow \infty$) uncorrelated over the frequency (cumulant mixing of order infinity).
- 6) $\text{var}(Y_S(k))$ is a continuous function of the frequency with continuous (higher order) derivatives.

where the expected values are taken w.r.t. the random input $u(t)$ (see [1], [17], and [18]). These first- and second-order properties are very similar to those of filtered white noise disturbances (see [17] and [19]), and therefore, it is very hard to distinguish the stochastic NL distortions $y_s(t)$ from the disturbing noise in frequency response function measurements. It motivates the equivalent scheme in Fig. 2, where $y_s(t)$ is represented as a disturbance.

B. Closed-Loop Case

The key difference between the closed-loop configuration (see Fig. 1) and the open-loop setup (see Fig. 2) is that, due to the feedback loop, the input $u(t)$ depends on the NL distortions produced by the system. Therefore, definition (1) leads to biased estimates of the BLA for NL systems operating in feedback. Indeed, assuming that we observe the steady-state response to a random phase multisine, we have that $Y(k) = G_{\text{BLA}}(j\omega_k)U(k) + Y_S(k)$. Hence, (1) becomes

$$\frac{S_{yu}(j\omega_k)}{S_{uu}(j\omega_k)} = \frac{\mathbb{E}\{Y(k)\bar{U}(k)\}}{\mathbb{E}\{|U(k)|^2\}} = G_{\text{BLA}}(j\omega_k) + \frac{\mathbb{E}\{Y_S(k)\bar{U}(k)\}}{\mathbb{E}\{|U(k)|^2\}}$$

where $\mathbb{E}\{Y_S(k)\bar{U}(k)\} \neq 0$ due to the feedback loop (see Appendix A).

Following the lines of [15] and [16] for identifying linear systems in closed loop, we redefine the BLA via the indirect method as

$$G_{\text{BLA}}(j\omega) = \frac{S_{yr}(j\omega)}{S_{ur}(j\omega)} = \frac{F\{\mathbb{E}\{y(t)r(t-\tau)\}\}}{F\{\mathbb{E}\{u(t)r(t-\tau)\}\}} \quad (3)$$

with $r(t)$ being the known reference signal (typically the signal stored in the arbitrary waveform generator), and where the expected values $\mathbb{E}\{\cdot\}$ are taken w.r.t. the random realization of $r(t)$. To study the properties of (3), we need the following assumption.

Assumption: The single-input two-output (SITO) open-loop system from reference $r(t)$ to input–output $z(t) = [y(t) u(t)]^T$ is an NL PISPO system.

Under this assumption, it is shown in Appendix B that the equivalence in Fig. 2, where $G_{\text{BLA}}(j\omega)$ is defined as in (3), can be applied to the NL system in Fig. 1: All properties of $y_s(t)$ ($Y_S(k)$) of the open-loop case (see Section II-A) remain valid except that $y_s(t)$ ($Y_S(k)$) is uncorrelated with the reference signal $r(t)$ ($R(k)$) instead of the input $u(t)$ ($U(k)$).

Define now $\tilde{U}_S(k)$ and $\tilde{Y}_S(k)$ as those parts of the input–output DFT spectra that are uncorrelated with $R(k)$. The difference $Y_S(k)$ between the actual output of the NL system and the output predicted by the BLA (3) is related to these observed input–output NL distortions $\tilde{U}_S(k)$ and $\tilde{Y}_S(k)$ as

$$Y_S(k) = \tilde{Y}_S(k) - G_{\text{BLA}}(j\omega_k)\tilde{U}_S(k) \quad (4)$$

(see Appendix B). According to the particular case, the actual output distortions $|Y_S(k)|$ produced by the NL system can be (much) larger or (much) smaller than the observed output distortions $|\tilde{Y}_S(k)|$. Examples are given in the sequel of this section.

The following properties of the BLA show that the new definition (3) is a natural extension of (1).

Properties of the BLA (3):

- 1) *Open Loop, NL System, and Linear Actuator:* If the NL system operates in open loop and the actuator is linear, then (3) reduces to (1) (proof: use $S_{yr}(j\omega) = S_{yu}(j\omega)/G_{\text{act}}(j\omega)$ and $S_{ur}(j\omega) = S_{uu}(j\omega)/G_{\text{act}}(j\omega)$, with $G_{\text{act}}(j\omega)$ being the actuator FRF, and where \bar{x} is the complex conjugate of x).

- 2) *Closed Loop, Linear System, NL Actuator, and NL Feedback*: If the system is linear and the actuator and/or feedback dynamics are NL, then the BLA (3) is equal to the FRF $G(j\omega_k)$ and $Y_S(k) = 0$ (proof: see Appendix C). This is an example where $|Y_S(k)|$ (4) is much smaller than $|\tilde{Y}_S(k)|$.
- 3) *Closed Loop, NL System, NL Actuator, and NL Feedback*: Since the proof in Appendix B does not use the linearity of the actuator and the feedback dynamics, the properties of $Y_S(k)$ remain valid for the NL actuator and/or feedback dynamics. For example, $Y_S(k)$ is still uncorrelated with $\tilde{R}(k)$, and the linear correction for the input NL distortions (4) is still exact without any approximation.

Interpretation of the Output Residual (4): Assuming that the actuator and the feedback are linear, the input–output DFT spectra of the NL system in Fig. 1 can be written as

$$\begin{aligned} Y(k) &= G_{\text{BLA}}(j\omega_k)U_R(k) + \tilde{Y}_S(k) + T_Y(j\omega_k) \\ U(k) &= U_R(k) + \tilde{U}_S(k) + T_U(j\omega_k) \end{aligned} \quad (5)$$

with $U_R(k)$ being that part of the input that is correlated with the reference signal

$$U_R(k) = \frac{G_{\text{act}}(j\omega_k)}{1 + G_{\text{BLA}}(j\omega_k)M(j\omega_k)}R(k) \quad (6)$$

where $G_{\text{act}}(j\omega)$ and $M(j\omega)$ stand for the actuator and feedback dynamics, respectively. $T_U(j\omega)$ and $T_Y(j\omega)$ represent the input–output transient (leakage) errors due to the DFT. These leakage errors are rational functions of the frequency that decrease as $O(N^{-1/2})$ w.r.t. the main terms as the number of time domain samples N increases to infinity [17], [20], [21]. The input–output stochastic NL distortions $\tilde{U}_S(k)$ and $\tilde{Y}_S(k)$ in (10) are related to $Y_S(k)$ in Fig. 2 as

$$\tilde{Y}_S(k) = \frac{Y_S(k)}{1 + G_{\text{BLA}}(j\omega_k)M(j\omega_k)} \quad (7)$$

$$\tilde{U}_S(k) = \frac{-Y_S(k)M(j\omega_k)}{1 + G_{\text{BLA}}(j\omega_k)M(j\omega_k)}. \quad (8)$$

Note that $\tilde{Y}_S(k)$ (7) and $\tilde{U}_S(k)$ (8) satisfy (4). Note also that $|Y_S(k)|$ (4) is much larger than $|\tilde{Y}_S(k)|$ if the open-loop gain $|G_{\text{BLA}}(j\omega_k)M(j\omega_k)|$ is much larger than one. It illustrates that a linear feedback loop combined with a high open-loop gain linearizes the NL behavior of the PISPO system.

III. MEASURING THE BLA

Consider the setup of Fig. 3 where the reference signal $r(t)$ is a random phase multisine

$$r(t) = \sum_{k=-N/2+1}^{N/2-1} R_k e^{j2\pi f_s k t / N} \quad (9)$$

with $R_k = \bar{R}_{-k} = |R_k|e^{j\angle R_k}$, f_s being the clock frequency of the arbitrary waveform generator, and N being the number of samples in one signal period. The amplitudes $|R_k|$ of the Fourier coefficients are deterministic and user defined (usually

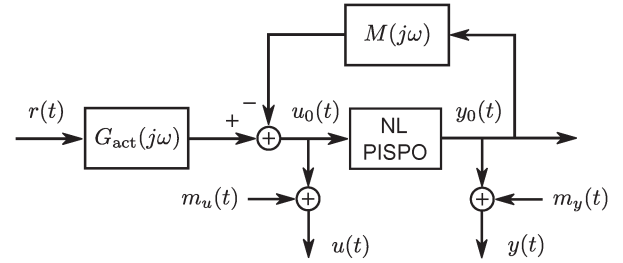


Fig. 3. Setup for measuring the BLA of an NL PISPO system operating in closed loop. $G_{\text{act}}(j\omega)$ and $M(j\omega)$ represent respectively the linear actuator and feedback dynamics. $m_u(t)$ and $m_y(t)$ are respectively the input and output measurement errors.

$R_0 = 0$), and the phases are randomly chosen over k such that $\mathbb{E}\{e^{j\angle R_k}\} = 0$, for example, a uniform distribution over $[0, 2\pi)$. The results presented in the sequel of this section are valid for multisines with a “sufficient” number of nonzero harmonics F such that $r(t)$ resembles Gaussian noise [1], [7], [17]. To keep the RMS value of the multisines (9) constant as $F = O(N) \rightarrow \infty$, the Fourier coefficients are scaled such that $|R_k| = O(N^{-1/2})$.

To avoid the transient (leakage) errors due to the system dynamics in (5), the acquisition channels and the arbitrary waveform generator are synchronized, and an integer number of periods of the steady-state response is measured. Hence, the measured input–output DFT spectra can be written as

$$\begin{aligned} Y(k) &= G_{\text{BLA}}(j\omega_k)U_R(k) + \tilde{Y}_S(k) + M_Y(k) \\ U(k) &= U_R(k) + \tilde{U}_S(k) + M_U(k) \end{aligned} \quad (10)$$

with $M_U(k)$ and $M_Y(k)$ being the input–output measurement errors, and where $\tilde{U}_S(k)$ and $\tilde{Y}_S(k)$ are defined in (8). Note that the transient (leakage) errors due to the noise dynamics have been neglected in (10). In those applications where this is not permitted (e.g., lowly damped vibrating mechanical structures), the noise leakage errors are suppressed nonparametrically as explained in [22].

In the sequel of this section, we summarize briefly the robust and the fast measurement procedure and discuss their properties; the reader is referred to [9], [12], and [17] for the details.

A. Robust Method

First, $P \geq 2$ periods of the steady-state response to a random phase multisine (9) are measured, and this experiment is repeated for $M \geq 4$ (or 7) independent random phase realizations (following the lines of [22], the minimal number of realizations M can be reduced to two). Next, the noisy input–output DFT spectra are analyzed over the P periods (step 1) and the M realizations (step 2).

Step 1) Calculate for each realization the sample means and sample (co)variances of the input–output DFT spectra over the periods. The result is a set of M sample means $\hat{U}^{[m]}(k)$ and $\hat{Y}^{[m]}(k)$, $m = 1, 2, \dots, M$, and an estimate of the corresponding input–output noise (co)variances.

Step 2) Before calculating the sample means and sample (co)variances over the M realizations, the mean input–output DFT spectra over the periods, $\hat{U}^{[m]}(k)$ and $\hat{Y}^{[m]}(k)$, must be referred to the reference signal as

$$\begin{aligned}\hat{Y}_R^{[m]}(k) &= \hat{Y}^{[m]}(k)e^{-j\angle R^{[m]}(k)} \\ \hat{U}_R^{[m]}(k) &= \hat{U}^{[m]}(k)e^{-j\angle R^{[m]}(k)}.\end{aligned}\quad (11)$$

Combining (11) with (10) shows that the sample means and sample (co)variances over the M realizations of $\hat{U}_R^{[m]}(k)$ and $\hat{Y}_R^{[m]}(k)$ result in an estimate of the BLA

$$\hat{G}_{\text{BLA}}(j\omega_k) = \frac{\frac{1}{M} \sum_{m=1}^M \hat{Y}_R^{[m]}(k)}{\frac{1}{M} \sum_{m=1}^M \hat{U}_R^{[m]}(k)} \quad (12)$$

and its total variance (sum noise variance and variance of the stochastic NL distortions). Subtracting the noise variance obtained in step 1 from the total variance gives an estimate of the variance of the stochastic NL distortions.

In Appendix D, it is shown that (12) is a consistent ($M \rightarrow \infty$) estimate of the BLA (3).

B. Fast Method

The fast method uses full (all harmonics are excited) or odd (only the odd harmonics are excited) random phase multisinuses $r(f)$ (9) with a random harmonic grid. The random harmonic grid is constructed as follows: The excited harmonics are split in groups of N_{sub} consecutive (odd) harmonics, and within each group, one randomly selected harmonic is not excited. By choosing N_{sub} , one makes a tradeoff between the effective frequency resolution of the BLA measurement ($(N_{\text{sub}} - 1)/N_{\text{sub}} \times f_{\text{res}}$) and the frequency resolution of the NL detection $f_{\text{res}}/N_{\text{sub}}$, where $f_{\text{res}} = f_s/N$ and $f_s/(2N)$ for full and odd multisinuses, respectively. Typical values for N_{sub} are 2, 3, or 4. These multisinuses are the Riemann equivalent with the full random phase multisinuses used in the robust method, which means that they lead to the same BLA with the Riemann equivalent variance of the stochastic NL distortions (see [7] for the details). The harmonics that are not excited in $r(t)$ are called detection lines.

Starting from $P \geq 4$ (or 7) periods of the steady-state response to one full (odd) random phase multisine with a random harmonic grid, the fast method estimates the BLA, its noise variance, and the variance of the stochastic NL distortions (following the lines of [22], the minimal number of periods can be reduced to two).

Step 1) Calculate the sample means and sample (co)variances of the input–output DFT spectra over the P periods. The result is the sample means $\hat{U}(k)$ and $\hat{Y}(k)$ and an estimate of the corresponding

input–output noise (co)variances. At the excited harmonics k_e , we calculate the BLA

$$\hat{G}_{\text{BLA}}(j\omega_{k_e}) = \frac{\hat{Y}(k_e)}{\hat{U}(k_e)} \quad (13)$$

and its noise variance.

Step 2) Select the nonexcited (odd) harmonics k_{ne} in the input–output DFT spectra and use (4) to estimate the stochastic NL distortions $Y_S(k)$

$$\hat{Y}_S(k_{\text{ne}}) = \hat{Y}(k_{\text{ne}}) - \hat{G}_{\text{BLA}}(j\omega_{k_{\text{ne}}})\hat{U}(k_{\text{ne}}) \quad (14)$$

where $\hat{G}_{\text{BLA}}(j\omega_{k_{\text{ne}}})$ is obtained via linear interpolation of $\hat{G}_{\text{BLA}}(j\omega_{k_e})$ (13). Next, the total variance (sum noise variance and variance of the stochastic NL distortions) of the BLA estimate $\hat{G}_{\text{BLA}}(j\omega_{k_e})$ is calculated as

$$\frac{|\hat{Y}_S(k_e)|^2}{|\hat{U}(k_e)|^2} \quad (15)$$

where $|\hat{Y}_S(k_e)|^2$ is obtained via linear interpolation of $|\hat{Y}_S(k_{\text{ne}})|^2$ at the nearest (odd) nonexcited harmonics.

For piecewise linearly varying BLAs, $|\hat{Y}_S(k_{\text{ne}})|^2$ is an unbiased estimate of the total variance (proof: see Appendix E). This motivates the calculation of the total variance of the BLA as in (15).

C. Comparison Fast and Robust Methods

The bias in the estimate (14) introduced by $\hat{G}_{\text{BLA}}(j\omega_{k_{\text{ne}}})$ can be neglected if the input-signal-to-distortion and input-signal-to-noise ratios are larger than 10 dB and if the frequency resolution is sufficiently large (proof: see Appendix E). Under these conditions, the total variance of the BLA predicted by the fast method coincides with that of the robust method. Note that the robust method does not need the assumption of a sufficiently large input-signal-to-distortion ratio. The robust method also does not require nonexcited harmonics in the reference signal, which results in a $N_{\text{sub}}/(N_{\text{sub}} - 1)$ or $2N_{\text{sub}}/(N_{\text{sub}} - 1)$ times larger frequency resolution of the BLA estimate. Moreover, the frequency resolution of the BLA estimate and the NL detection are the same for the robust method.

D. NL Actuator and/or Feedback Dynamics

If the actuator and/or the feedback dynamics are NL, then the linear compensation (14) of the output DFT spectrum for the input distortions is still valid because the proof in Appendix B does not use the linearity of the actuator and feedback dynamics.

If the plant is linear, then the NL distortions produced by the actuator and/or the feedback act as generator noise: The estimated BLA is equal to the linear plant dynamics, and its total variance only depends on the input–output noise (co)variances (proof: see Appendix C).

E. Measurement of the Feedback Dynamics

Consider the setup of Fig. 1 where the actuator and the feedback are linear. For NL systems, the frequency response function calculated at the nonexcited harmonics equals minus one over the feedback dynamics. Indeed, assuming that no input–output measurement noise is present, the input–output DFT spectra are related as [17]

$$U(k) = G_{\text{act}}(j\omega_k)R(k) - M(j\omega_k)Y(k) \quad (16)$$

where $G_{\text{act}}(j\omega_k)$ and $M(j\omega)$ stand for the actuator and feedback dynamics, respectively. Evaluating (16) at the nonexcited harmonics gives

$$U(k_{\text{ne}}) = -M(j\omega_{k_{\text{ne}}})Y(k_{\text{ne}}) \quad (17)$$

which proves the statement. Note that $U(k_{\text{ne}}) = \tilde{U}_S(k_{\text{ne}})$ and $Y(k_{\text{ne}}) = \tilde{Y}_S(k_{\text{ne}})$, where $\tilde{U}_S(k)$ and $\tilde{Y}_S(k)$ are defined in (8). It shows that the feedback dynamics can be measured at the nonexcited harmonics because of the NL distortions $y_s(t)$ (replace the NL PISPO system in Fig. 3 by its equivalent scheme in Fig. 2).

IV. DETECTION, CLASSIFICATION, AND QUANTIFICATION OF THE EVEN AND ODD NONLINEARITIES

Using odd random phase multisines with a random harmonic grid, the frequency response function measurement of an NL system operating in *open loop* and driven by a *linear actuator* can be fully characterized: Aside from the estimates of the BLA, its noise variance, and its total variance, also the level of the odd and even NL distortions is quantified (see [9]). The latter gives some physical insight into the NL behavior and is useful for designing better experiments. For example, if it turns out that the odd or the even distortions are dominant, then the variability of the BLA measurement can be reduced (significantly) by using periodic signals that excite respectively all harmonics or only the odd harmonics (see [17]). The fast method discussed in Section III-B extracts this information from one single experiment. For NL actuators or NL systems operating in a *closed-loop* configuration, the fast method still estimates the correct BLA and its noise and total variances, provided that the input-signal-to-distortion ratio is sufficiently large (e.g., > 10 dB). However, the estimated level of the even and odd NL distortions might be biased. This is illustrated in the sequel of this section.

A. Conditions for Unbiased Estimation of the Level of the Even and Odd Distortions

Consider an open-loop NL PISPO system (see Fig. 2) consisting of the cascade of a static nonlinearity $z(t) = \alpha u^2(t) + \beta u^3(t)$ and a linear dynamic system $G(j\omega)$. Since $u^2(t)$ and $u^3(t)$ combine respectively two and three frequencies of $u(t)$,

the dominant stochastic NL contributions at the even detection lines in $z(t)$ are of the form

$$\begin{aligned} \alpha u^2(t) &: \alpha U(2k_1 + 1)U(2k_2 + 1) \\ \beta u^3(t) &: \beta U(2k_3 + 1)U(2k_4 + 1)U(2l) \end{aligned} \quad (18)$$

with $2k_1 + 2k_2 + 2 = 2m$ and $2k_3 + 2k_4 + 2l + 2 = 2m$. $U(2k_i + 1)$, $i = 1, \dots, 4$, denotes the excited harmonics, and $U(2l)$ denotes an even distortion line. If $|\beta U(2l)|$ is not much smaller than $|\alpha|$, then the third degree contribution in (18) will bias the estimated level of the even NL distortions. As a rule of thumb, this bias can be neglected if the ratio of the power spectra (power spectral densities) of the odd to the even NL distortions is much smaller than the ratio of the power spectra (power spectral densities) of the odd excited harmonics to the even distortion lines

$$\frac{S_{y_s y_s, \text{odd}}(j\omega)}{S_{y_s y_s, \text{even}}(j\omega)} \ll \frac{S_{uu, \text{odd}}(j\omega)}{S_{uu, \text{even}}(j\omega)} \Rightarrow \text{no bias even dist.} \quad (19)$$

(see Appendix F for a rationale). The relationship between the DFT spectrum and the power spectral density is given by

$$\begin{aligned} S_{xx, \text{odd}}(j\omega_{2k+1}) &= \frac{\mathbb{E}\{|X(2k+1)|^2\}}{2f_s} + O(N^{-1}) \\ S_{xx, \text{even}}(j\omega_{2k}) &= \frac{\mathbb{E}\{|X(2k)|^2\}}{2f_s} + O(N^{-1}) \end{aligned} \quad (20)$$

with $x(t) = u(t)$, $y_s(t)$ and $X(k) = U(k)$, $Y_S(k)$, where the factor 2 accounts for the frequency resolution of the even and odd DFT lines. Note that the expected values are taken w.r.t. the random phase realizations and the random grid of the odd random phase multisine $r(t)$ with random harmonic grid (e.g., $\mathbb{E}\{|R(2k+1)|^2\} = (N_{\text{sub}} - 1)/N_{\text{sub}}|R(2k_e + 1)|^2$).

Similarly, the dominant stochastic NL contributions at the odd detection lines $2m + 1$ in $z(t)$ (odd nonexcited harmonics in $r(t)$) are of the type

$$\begin{aligned} \alpha u^2(t) &: \alpha U(2k_1 + 1)U(2l) \\ \beta u^3(t) &: \beta U(2k_2 + 1)U(2k_3 + 1)U(2k_4 + 1) \end{aligned} \quad (21)$$

with $U(2k_i + 1)$, $i = 1, \dots, 4$, being the excited harmonics and $U(2l)$ being an even distortion line. If $|\alpha U(2l)|$ is not much smaller than $|\beta U(2k_2 + 1)U(2k_3 + 1)|$, then the even NL contribution in (21) will bias the estimated level of the odd NL distortions. As a rule of thumb, this bias can be neglected if

$$\frac{S_{y_s y_s, \text{even}}(j\omega)}{S_{y_s y_s, \text{odd}}(j\omega)} \ll \frac{S_{uu, \text{odd}}(j\omega)}{S_{uu, \text{even}}(j\omega)} \Rightarrow \text{no bias odd dist.} \quad (22)$$

is satisfied (see Appendix F for a rationale).

B. Discussion

The bias on the estimated levels of the even and odd NL distortions can be neglected if the even and odd distortions are of the same order of magnitude ($S_{y_s y_s, \text{even}}(j\omega) \sim S_{y_s y_s, \text{odd}}(j\omega)$) and if the input-signal-to-even-distortion ratio is sufficiently large ($S_{uu, \text{odd}}(j\omega)/S_{uu, \text{even}}(j\omega) \gg 1$). If, for example, the even distortions are dominant ($S_{y_s y_s, \text{even}}(j\omega) \gg$

$S_{y_s y_s, \text{odd}}(j\omega)$), then (19) is automatically satisfied and the level of the even NL distortions is correctly estimated. However, the unbiased estimation of the level of the odd distortions puts a severe constraint on the input-signal-to-even-distortion ratio [see (22)]. If the odd distortions are dominant, then the opposite is true: The level of the odd NL distortions is correctly estimated, while the unbiased estimation of the level of the even distortions puts a strong condition on the input-signal-to-even-distortion ratio [see (19) with $S_{y_s y_s, \text{even}}(j\omega) \ll S_{y_s y_s, \text{odd}}(j\omega)$]. These results are also valid for NL systems operating in feedback. Note that conditions (19) and (22) can easily be checked *a posteriori*.

V. SIMULATION EXAMPLE

The goal of the simulation example is threefold: 1) the illustration of the influence of the spectral impurity of the odd random phase multisine on the predicted levels of the odd and even NL distortions; 2) the verification of conditions (19) and (22) for the unbiased estimation of the levels of the even and odd distortions; and 3) the comparison of the robust and fast methods for measuring the BLA using spectrally impure odd random phase multisines.

A. Simulation Setup

For the simulation, we use the setup of Fig. 1 without feedback loop (open-loop operation), where the actuator is a fourth-order analog Chebyshev filter with a passband ripple of 6 dB and a cutoff frequency of 2 kHz and where the NL PISPO system is a Wiener–Hammerstein system consisting of the cascade of a first linear dynamic system $G_1(s)$, a static NL system $z(t) = f(x(t))$, and a second linear system $G_2(s)$

$$G_1(s) = \frac{1}{1 + s/(Q\omega_0) + s^2/\omega_0^2} \quad (23)$$

$$f(x(t)) = x(t) + 0.01x^2(t) + \beta x^3(t) \quad (24)$$

$$G_2(s) = \frac{1}{1 + \tau s} \quad (25)$$

with $Q = 10$, $\omega_0 = 2\pi f_0$, $f_0 = 1$ kHz, and $\tau = 1/(600\pi)$ s. The reference signal $r(t)$ is an odd random phase multisine with a random harmonic grid covering the band [4 Hz, 2 kHz] with a frequency resolution of 4 Hz, an RMS value equal to one, and $N_{\text{sub}} = 2$ (one out of two consecutive odd harmonics is randomly eliminated). Two different Wiener–Hammerstein systems are simulated: the first having a dominant odd behavior ($\beta = 5 \times 10^{-3}$) and the second having a dominant even behavior ($\beta = 5 \times 10^{-4}$). We choose $f_s = 50$ kHz and disturb the input–output signals at the sampling instances by normally distributed white noise with zero mean and standard deviation 1×10^{-4} . The fast method of Section III-B is applied to $P = 2$ consecutive periods of the steady-state response to the following two odd random phase multisines with the same RMS value (Riemann equivalent power spectrum):

- 1) undistorted odd multisine: no signal energy at the odd nonexcited harmonics (= the original reference signal $r(t)$);

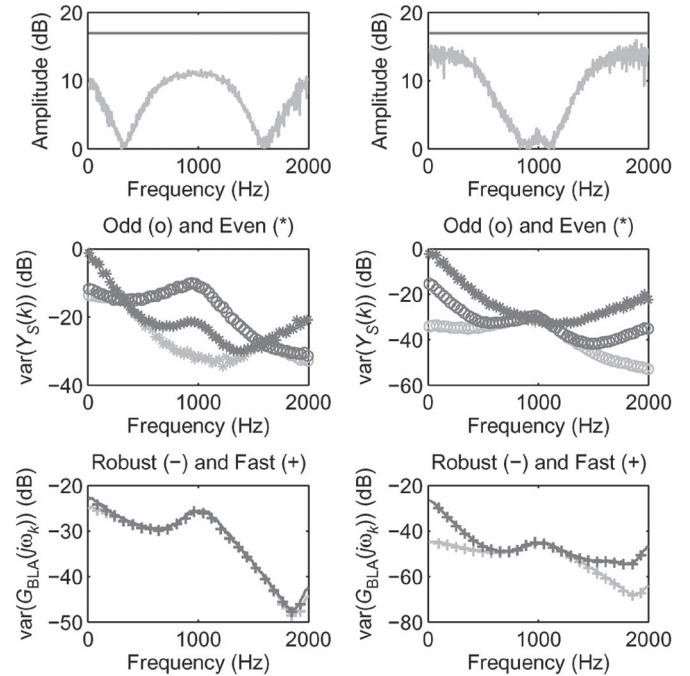


Fig. 4. Quantification of the even and odd NL distortions using odd random phase multisines with random harmonic grid—Wiener–Hammerstein simulation example. Top row: Comparison between (dark gray) $S_{uu, \text{odd}}/S_{uu, \text{even}}$ and, respectively, (left plot, light gray) $S_{y_s y_s, \text{odd}}/S_{y_s y_s, \text{even}}$ and (right plot, light gray) $S_{y_s y_s, \text{even}}/S_{y_s y_s, \text{odd}}$. Middle and bottom rows: Estimated level of the stochastic NL distortions on (Y_S , middle row) the output and (G_{BLA} , bottom row) the BLA for the (light gray) undistorted and (dark gray) distorted odd multisines. Left column: $\alpha = 0.01$ and $\beta = 5 \times 10^{-3}$. Right column: $\alpha = 0.01$ and $\beta = 5 \times 10^{-4}$.

- 2) even distorted odd multisine: no signal energy at the odd detection lines and signal energy at the even in-band harmonics with a constant amplitude that is ten times smaller than the excited odd harmonics and a random phase that is uniformly distributed in $[0, 2\pi)$ (= the original reference signal $r(t)$ + an even distortion).

In order to have a smooth estimate of the level of the NL distortions, the whole procedure is repeated for $M = 1000$ independent random phase realizations of the odd multisines, and the mean values over these realizations of the estimated variance of the even $|\hat{Y}_S(2k)|^2$ and odd $|\hat{Y}_S(2k_{\text{ne}} + 1)|^2$ NL distortions (14) and of the estimated variance $|\hat{Y}_S(2k_e + 1)|^2/|U(2k_e + 1)|^2$ of the BLA are calculated. In addition, it allows to compare the fast (see Section III-B) to the robust (see Section III-A) estimates.

B. Simulation Results

The simulations with the undistorted multisine result in the unbiased estimates of the levels of the even and odd NL distortions and serve as a reference for the simulations with the distorted odd multisine. Fig. 4 shows the results. The following can be observed.

- 1) In the first example (see Fig. 4, left column), the Wiener–Hammerstein with $\beta = 5 \times 10^{-3}$ in (24) has a dominant odd NL behavior, and the even distorted odd multisine overestimates the level of the even NL distortions in the band [500 Hz, 1200 Hz].

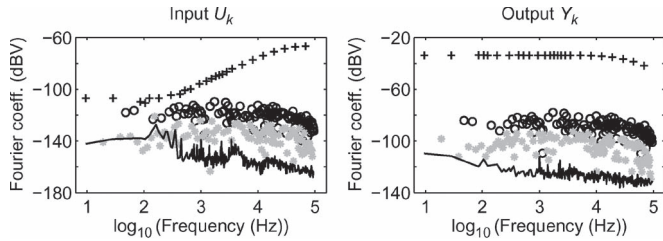


Fig. 6. Measured (left) input and (right) output Fourier coefficients of the opamp excited by an odd random phase multisine with a logarithmic random harmonic grid (not all excited and nonexcited frequencies are shown). “+”: excited odd harmonic; “o”: nonexcited odd harmonic; “gray *”: nonexcited even harmonics; and black line noise variance (all harmonics).

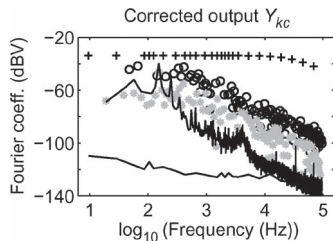


Fig. 7. Corrected output Fourier coefficients (26) of the opamp (not all harmonics are shown). “+”: excited odd harmonics; “o”: odd nonexcited harmonics; “gray *”: even nonexcited harmonics; bottom black line: noise variance excited harmonics; and top black line: noise variance nonexcited harmonics.

mean value of the Fourier coefficients (excited and nonexcited harmonics). The following observations can be made.

- 1) The odd (o) and even (gray *) nonexcited harmonics are well above the noise level (black line), except the even input harmonics below 200 Hz.
- 2) The odd nonexcited harmonics (o) are significantly larger than the even nonexcited harmonics (gray *).
- 3) The output distortions (see Fig. 6, right plot) are about 50 dB (o) to 70 dB (gray *) below the linear contributions.

Although it is tempting to conclude from observation 2 that the opamp has a dominant odd NL behavior, one needs to verify first whether (22) is fulfilled before drawing this conclusion. From observation 3, one could wrongly conclude that the opamp behaves fairly linearly. This is due to the linearizing effect of the feedback loop in the test circuit (resistor R_2 in Fig. 5).

The linear compensation (14) of the output Fourier coefficients for the parasitic power at the nonexcited input harmonics gives the corrected output Fourier coefficients Y_{ck}

$$Y_{ck} = \frac{Y_c(k)}{\sqrt{N}} \quad \text{with} \quad \begin{cases} Y_c(k_e) = Y(k_e) \\ Y_c(k_{ne}) = \hat{Y}_S(k_{ne}) \end{cases} \quad (26)$$

shown in Fig. 7. The horizontal and oblique black lines indicate the noise standard deviations of the excited and nonexcited harmonics, respectively. In addition to the previous observations, the following can be seen.

- 1) Below 10 kHz, the noise level of the nonexcited output harmonics is much larger after correction (compare the oblique and the horizontal black lines). This is due to the input noise and the high gain of the opamp.

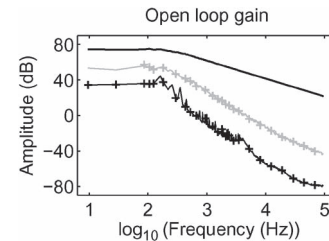


Fig. 8. Comparison between the (solid lines) robust and (“+”) fast estimates of the open-loop gain. Black line: Open-loop gain (both estimates coincide). Thin black line and “black +”: Noise variance. Gray line and “gray +”: Total variance (noise + NL distortion).

- 2) The NL distortions in the corrected output spectrum are much larger than that in the original output spectrum (compare Figs. 6 and 7). Hence, the linear correction (14) opens the feedback loop.

In order to verify that the level of the odd NL distortions in the compensated output spectrum (see Fig. 7) quantifies correctly the level of the NL distortions on the BLA measurement, the results of the fast method (see Section III-B) are compared to those of the robust method (see Section III-A). Therefore, the fast method is applied to each of the $M = 25$ experiments, and the mean value of the BLA, its noise, and total variances are calculated over these 25 estimates. From Fig. 8, it can be seen that the fast and robust estimates coincide. It nicely illustrates that the linear compensation (14) for the spectral impurity of the input in the fast method is correct.

C. Classification and Quantification of the Even and Odd Nonlinearities

Although the odd NL distortions in the compensated output spectrum (see Fig. 7) quantify correctly the variability of the BLA measurement (see Fig. 8), the relationship between the true even and odd NL behavior of the opamp and the level of the even and odd nonexcited harmonics in the corrected output spectrum is valid only if inequalities (19) and (22) are satisfied. The power spectral densities in inequalities (19) and (22) are calculated via (20), where the expected values are approximated by the mean value of $|\hat{U}(k)|^2$ and $|\hat{Y}_S(k_{ne})|^2$ (14) over the 25 experiments. Fig. 9 shows the power ratios $S_{uu,odd}/S_{uu,even}$ (black), $S_{y_s y_s, odd}/S_{y_s y_s, even}$ (light gray), and $S_{y_s y_s, even}/S_{y_s y_s, odd}$ (dark gray) as a function of the logarithm of the frequency. The following conclusions can be drawn.

- 1) Over the whole frequency band, $S_{y_s y_s, even}/S_{y_s y_s, odd}$ (dark gray) is much smaller than $S_{uu, odd}/S_{uu, even}$ (black) so that inequality (22) is fulfilled. Hence, the level of the odd nonexcited harmonics in the corrected output spectrum (see Fig. 7, “o”) is a correct indication of the level of the odd NL distortions.
- 2) Above 1 kHz, the power ratio $S_{y_s y_s, odd}/S_{y_s y_s, even}$ (light gray) is much smaller than $S_{uu, odd}/S_{uu, even}$ (black) so that inequality (19) is satisfied. Hence, the level of the even nonexcited harmonics in the corrected output spectrum (see Fig. 7, “gray *”) is a correct indication of the level of the even NL distortions. This is no longer true in

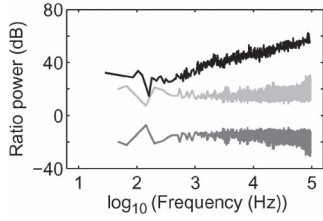


Fig. 9. Comparison between the (black) input-signal-to-even-distortion power ratio $S_{uu,odd}/S_{uu,even}$ and the power ratio of the (dark gray) even to the odd $S_{y_s y_s,even}/S_{y_s y_s,odd}$ and the (light gray) odd to the even $S_{y_s y_s,odd}/S_{y_s y_s,even}$ distortions.

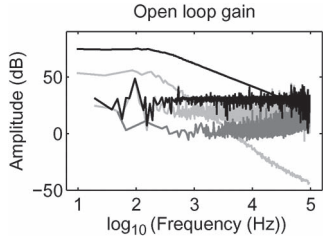


Fig. 10. Frequency response function evaluated at the (top black line) excited and (horizontal black line) nonexcited harmonics and the corresponding total variances (top light gray line: excited harmonics; horizontal dark gray line: nonexcited odd harmonics; and horizontal light gray line: nonexcited even harmonics).

the band [200 Hz, 1 kHz]. Below 200 Hz, the even output harmonics are at the noise level (see Fig. 7).

D. Measurement of the Feedback Dynamics

For each of the $M = 25$ experiments, the BLA is also calculated at the nonexcited frequencies k_{ne}

$$\hat{G}_{BLA}^{[m]}(j\omega_{k_{ne}}) = \frac{\hat{Y}^{[m]}(k_{ne})}{\hat{U}^{[m]}(k_{ne})} \quad (27)$$

where $\hat{X}^{[m]}(k)$, $X = U, Y$, are the mean input–output DFT spectra over the $P = 5$ periods, with $m = 1, 2, \dots, M$. The sample mean and sample variance of (27) over the $M = 25$ experiments are shown in Fig. 10 (horizontal black and gray lines). The following observations can be made.

- 1) The variance of the BLA at the nonexcited odd harmonics is significantly smaller than that at the nonexcited even harmonics. The explanation follows immediately from Fig. 6: The input–output odd-distortion-to-noise levels are about 20 dB larger than the input–output even-distortion-to-noise levels.
- 2) Calculating the mean value of the estimated BLA over the nonexcited frequencies (black horizontal line in Fig. 10) gives 30.5 dB. This should be compared to the theoretical expected value

$$-1/M(j\omega) = \frac{(R_1 + R_g + R_2)}{(R_1 + R_g)} \approx 31.0 \text{ dB}$$

(see (17) and Fig. 11, where R_2 includes the 50- Ω output impedance of the voltage buffer).

The second observation nicely illustrates the results of Section III-E.

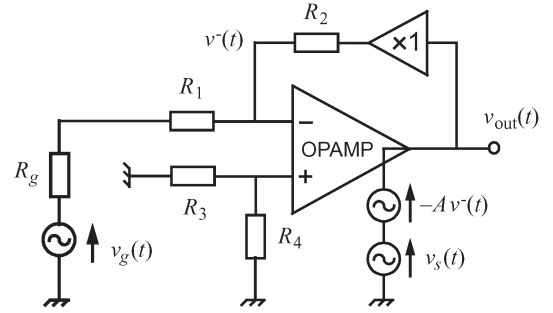


Fig. 11. Block schematic of the BLA of an opamp excited by a random phase multisine $v_g(t)$. The voltage source of the stochastic NL distortions $v_s(t)$ is uncorrelated with—but not independent of—the generator $v_g(t)$.

E. Discussion

Using the results of Section II-B, it follows immediately that the new opamp model (see Fig. 11) proposed in [10] is exact without any approximation. In this scheme (see Fig. 11), the open-loop gain A represents the BLA (3), and $v_s(t)$ represents the stochastic NL distortions that are uncorrelated with—but not independent of—the source voltage $v_g(t)$. Hence, the response (first-order moment) of the circuit to the voltage sources $v_g(t)$ and $v_s(t)$ and its variance (second-order moment) can be calculated using the superposition theorem. The part of $-Av^-(t)$ that is correlated with $v_g(t)$ contains energy at the excited harmonics only, while $v_s(t)$ has energy at all harmonics.

The open-loop gain and the variance of the stochastic NL distortions can be estimated using the fast (see Section III-B) or the robust (see Section III-A) method. At the nonexcited frequencies of $v_g(t)$, the voltage source $v_s(t)$ has nonzero power, and the BLA measurement equals minus one over the feedback dynamics (see (17)). The quality of the latter depends on the NL-distortion-to-noise ratio: The stronger the nonlinearity, the smaller the variance (see Fig. 10, horizontal gray lines).

VII. CONCLUSION

The definition of the BLA of an NL system has been generalized to the closed-loop case. For NL systems operating in open loop and excited by linear actuators, the generalized definition reduces to the classical one. The BLA of NL systems operating in closed loop can be measured using the existing robust and fast methods. At the nonexcited frequencies, one recovers minus one over the linear feedback dynamics. Hence, using specially designed periodic signals, it is possible to measure simultaneously the BLA and the linear feedback dynamics from a single experiment.

An absolute interpretation of the output NL distortions requires a linear compensation of the output spectrum for the spectral impurity of the input. It has been shown that this linear correction is exact without any approximation, even if the actuator and/or the feedback are NL. Although the corrected output spectrum quantifies exactly the variability of the BLA measurement, the levels of the even and odd nonexcited frequencies in the corrected output spectrum are unbiased estimates of the true even and odd NL behaviors only if some inequality constraints are satisfied. These constraints can be checked *a posteriori*.

Finally, the theory has been illustrated on open-loop gain measurements of an opamp. It follows that the new opamp model proposed in [10] is exact.

APPENDIX A

CORRELATION BETWEEN $Y_S(k)$ AND $U(k)$ FOR NL SYSTEMS OPERATING IN CLOSED LOOP

To simplify the notations, the arguments are omitted in this appendix. If the feedback dynamics are linear, then the input DFT spectrum U is related to the output of the actuator W and the NL distortions Y_S as (combine Figs. 1 and 2)

$$U = \frac{1}{1 + G_{BLA}M}W - \frac{M}{1 + G_{BLA}M}Y_S.$$

Hence, $\mathbb{E}\{Y_S\bar{U}\} = -\bar{M}/(1 + \overline{G_{BLA}M})\mathbb{E}\{|Y_S|^2\} \neq 0$. If the feedback dynamics are NL, then an explicit expression for $\mathbb{E}\{Y\bar{U}\}$ can be found using the results of Appendix B. Combining (28) and (32), it can easily be verified that $\mathbb{E}\{Y_S\bar{U}\} = \mathbb{E}\{\tilde{Y}_S\bar{\tilde{U}}_S\} - G_{BLA}\mathbb{E}\{\tilde{U}_S|^2\} \neq 0$, where \tilde{U}_S and \tilde{Y}_S are the observed input and output distortions, respectively.

APPENDIX B

BLA OF AN NL SYSTEM OPERATING IN CLOSED LOOP

To simplify the notations and without any loss of generality, we neglect the leakage errors in the DFT spectra. Consider now the closed-loop setup of Fig. 1, and define the open-loop system where $r(t)$ is the scalar input and $z(t) = [y(t) \ u(t)]^T$ is the vector of the two output signals. By assumption, this SITO open-loop system is an NL PISPO system. Applying definition (1) to this SITO system gives

$$Z(k) = G_{zr}(j\omega)R(k) + \tilde{Z}_S(k) \quad (28)$$

where $G_{zr}(j\omega)$ is the 2×1 BLA from $r(t)$ to $z(t)$, with $\tilde{Z}_S(k)$ being the 2×1 vector of the stochastic NL distortions that are uncorrelated with—but not independent of— $R(k)$ (proof: see [6] and [23]). Note that $\tilde{Z}_S(k)$ has exactly the same properties as $Y_S(k)$ in Section II-A, where $u(t)$ is replaced by $r(t)$, because both are the output distortions of an open-loop NL PISPO system. Combining (28) with

$$G_{rz}(j\omega) = \begin{bmatrix} G_{yr}(j\omega) \\ G_{ur}(j\omega) \end{bmatrix} = \begin{bmatrix} \frac{S_{yr}(j\omega)}{S_{rr}(j\omega)} \\ \frac{S_{ur}(j\omega)}{S_{rr}(j\omega)} \end{bmatrix} \quad (29)$$

$$\tilde{Z}_S(k) = \begin{bmatrix} \tilde{Y}_S(k) \\ \tilde{U}_S(k) \end{bmatrix}, \quad Z(k) = \begin{bmatrix} Y(k) \\ U(k) \end{bmatrix} \quad (30)$$

the difference $Y_S(k)$ between the actual output $Y(k)$ of the closed-loop system and the output predicted by the BLA (3) can be calculated as

$$Y_S(k) = Y(k) - G_{BLA}(j\omega_k)U(k) \quad (31)$$

$$= \tilde{Y}_S(k) - G_{BLA}(j\omega_k)\tilde{U}_S(k) \quad (32)$$

$$= [1 \quad -G_{BLA}(j\omega_k)]\tilde{Z}_S(k). \quad (33)$$

It shows that $Y_S(k)$ inherits all properties of $\tilde{Z}_S(k)$ (e.g., $Y_S(k)$ is uncorrelated with $R(k)$) which concludes the proof.

APPENDIX C

INFLUENCE OF THE ACTUATOR AND THE FEEDBACK DISTORTIONS ON THE FRF ESTIMATE

We consider here the setup of Fig. 1, where the actuator and/or the feedback are NL and where the plant is linear. To simplify the notations, we assume—without any loss of generality—that the input–output measurement errors are zero and that the reference signal $r(t)$ is a random phase multisine (9).

1) *BLA*: Applying the definition of the BLA (3) for NL systems operating in closed loop gives

$$G_{BLA}(j\omega) = \frac{S_{yr}(j\omega)}{S_{ur}(j\omega)} = \frac{G(j\omega)S_{ur}(j\omega)}{S_{ur}(j\omega)} = G(j\omega) \quad (34)$$

where the second equality uses the property that the plant has linear dynamics $G(j\omega)$.

2) *Output Residual*: Replacing $G_{BLA}(j\omega_k)$ by $G(j\omega_k)$ in (31) of Appendix B and taking into account that $Y(k) = G(j\omega_k)U(k)$ ($u(t)$ and $y(t)$ are periodic, and the system is linear) show that $Y_S(k) = 0$.

3) *Variance of the Estimated BLA*: Consider the robust (12) and fast (13) BLA estimates. Since the system is linear, we have that $\hat{Y}^{[m]}(k) = G(j\omega_k)\hat{U}^{[m]}(k)$ for all the random phase realizations $m = 1, 2, \dots, M$ of the random phase multisine (9) (by assumption, there is no input–output measurement noise). Hence, the BLA estimates (12) and (13) are equal to $G(j\omega_k)$ for all experiments, which implies that $\text{var}(G(j\omega_k)) = 0$. It shows that the stochastic NL distortions generated by the actuator and/or the feedback do not influence the variability of the FRF estimate.

APPENDIX D

THE ROBUST ESTIMATE OF THE BLA (12) IS CONSISTENT

Since the M experiments are independent, the sums in the numerator and denominator of (12) converge with probability 1 to their expected values as $M \rightarrow \infty$ (strong law of large numbers [24]). Hence, using (10), we find with probability 1

$$\begin{aligned} \lim_{M \rightarrow \infty} \hat{G}_{BLA}(j\omega_k) &= \frac{\mathbb{E}\left\{\hat{Y}^{[m]}(k)e^{-j\angle R^{[m]}(k)}\right\}}{\mathbb{E}\left\{\hat{U}^{[m]}(k)e^{-j\angle R^{[m]}(k)}\right\}} \\ &= \frac{\mathbb{E}\left\{\hat{Y}^{[m]}(k)\overline{R^{[m]}(k)}\right\}}{\mathbb{E}\left\{\hat{U}^{[m]}(k)\overline{R^{[m]}(k)}\right\}} \\ &= \frac{S_{yr}(j\omega_k)}{S_{ur}(j\omega_k)} \end{aligned}$$

which concludes the proof (the second equality uses the fact that $|R^{[m]}(k)|$ is deterministic and independent of m).

APPENDIX E

PROPERTIES OF THE RESIDUALS (14)

The bias in the fast BLA estimate (13) can be neglected if the input-signal-to-noise and signal-to-distortion ratios are larger

than 10 dB [17], [25]. If the BLA $G_{\text{BLA}}(j\omega)$ varies piecewise linearly over the frequency, then the linear interpolation does not introduce bias errors, and hence, $\mathbb{E}\{\hat{G}_{\text{BLA}}(j\omega_{k_{\text{ne}}})\} = G_{\text{BLA}}(j\omega_{k_{\text{ne}}})$. Note that the piecewise linearity condition is practically fulfilled for a sufficiently large frequency resolution. Using this result together with $\hat{Y}_0(k) = Y_0(k) + M_Y(k)$, $\hat{U}_0(k) = U_0(k) + M_U(k)$, $Y_S(k_{\text{ne}}) = Y_0(k_{\text{ne}}) - G_{\text{BLA}}(j\omega_{k_{\text{ne}}})U_0(k_{\text{ne}})$, and $N(k) = M_Y(k) - G_{\text{BLA}}(j\omega_k)M_U(k)$, the expected value of $|\hat{Y}_S(k_{\text{ne}})|^2$ is found to be

$$\begin{aligned} \mathbb{E}\left\{|\hat{Y}_S(k_{\text{ne}})|^2\right\} &= \mathbb{E}\left\{|Y_S(k_{\text{ne}})|^2\right\} + \mathbb{E}\left\{|N(k_{\text{ne}})|^2\right\} \\ &= \text{var}(Y_S(k_{\text{ne}})) + \text{var}(N(k_{\text{ne}})) \end{aligned} \quad (35)$$

which proves that $|\hat{Y}_S(k_{\text{ne}})|^2$ is an unbiased estimate of the total variance. As a consequence, subtracting an unbiased estimate of the noise variance from $|\hat{Y}_S(k_{\text{ne}})|^2$ results in an unbiased estimate of the variance of the stochastic NL distortions.

APPENDIX F RATIONALE FOR (19) AND (22)

The following two assumptions are made for deriving (19) and (22): (i) The phases of the plant input multisine are independently distributed, and (ii) the plant input-signal-to-even-distortion ratio is frequency independent. Assumption (i) is only approximately valid for NL systems operating in open loop and driven by an NL actuator and for NL systems operating in feedback (and driven by a linear actuator). In general, assumption (ii) will be an approximation too. Therefore, the reasoning in this appendix is a rationale and not a strict proof of inequalities (19) and (22).

1) *Rationale for (19)*: The bias on the estimated level of the even distortions can be neglected if the sum of all stochastic NL contributions of the form (18) satisfies

$$\begin{aligned} \left| \sum_{k_3, k_4} \beta U(2k_3 + 1)U(2k_4 + 1)U(2l) \right|^2 \\ \ll \left| \sum_{k_1} \alpha U(2k_1 + 1)U(2k_2 + 1) \right|^2 \end{aligned} \quad (36)$$

where l depends on k_3 and k_4 , k_2 depends on k_1 [see (18)], and

$$\sum_{k_1} \alpha U(2k_1 + 1)U(2k_2 + 1) = Y_{S,\text{even}}(2m) \quad (37)$$

(see [1] and [17]). We elaborate now the left-hand side of (36) assuming that the input-signal-to-even-distortion ratio $|U(2l + 1)|/|U(2l)|$ is independent of l and that the phases of the multisine $u(t)$ are independently distributed. The factor $U(2l)$ in the left-hand side of (36) can be rewritten as

$$\begin{aligned} U(2l) &= |U(2l + 1)| \frac{U(2l)}{|U(2l + 1)|} \\ &= |U(2l + 1)| e^{j\angle U(2l)} \frac{|U(2l)|}{|U(2l + 1)|}. \end{aligned} \quad (38)$$

Replacing $U(2l)$ in the left-hand side of (36) by (38) and taking into account that $|U(2l + 1)|/|U(2l)|$ is independent of l gives

$$\begin{aligned} \left| \sum_{k_3, k_4} \beta U(2k_3 + 1)U(2k_4 + 1)U(2l) \right|^2 &= \frac{|U(2m)|^2}{|U(2m + 1)|^2} \\ &\times \left| \sum_{k_3, k_4} \beta U(2k_3 + 1)U(2k_4 + 1)|U(2l + 1)| e^{j\angle U(2l)} \right|^2. \end{aligned} \quad (39)$$

Since the phases of $U(2l + 1)$ and $U(2l)$ are independently distributed, we can approximate the sum in the right-hand side of (39) as

$$\begin{aligned} \sum_{k_3, k_4} \beta U(2k_3 + 1)U(2k_4 + 1)|U(2l + 1)| e^{j\angle U(2l)} \\ \approx Y_{S,\text{odd}}(2m + 1). \end{aligned} \quad (40)$$

Collecting (36), (37), (39), and (40) and multiplying the result with $|U(2m + 1)|^2$, we find

$$|U(2m)|^2 |Y_{S,\text{odd}}(2m + 1)|^2 \ll |U(2m + 1)|^2 |Y_{S,\text{even}}(2m)|^2. \quad (41)$$

Taking the expected value of (41) and dividing by $\mathbb{E}\{|U(2m)|^2\}$ gives

$$\text{var}(Y_{S,\text{odd}}(2m + 1)) \ll \frac{\mathbb{E}\{|U(2m + 1)|^2\}}{\mathbb{E}\{|U(2m)|^2\}} \text{var}(Y_{S,\text{even}}(2m)). \quad (42)$$

Combining (20) with (42) finally proves (19).

2) *Rationale for (22)*: The bias on the estimated level of the odd distortions can be neglected if the sum of all stochastic NL contributions of the form (21) satisfies

$$\begin{aligned} \left| \sum_{k_1} \alpha U(2k_1 + 1)U(2l) \right|^2 \\ \ll \left| \sum_{k_2, k_3} \beta U(2k_2 + 1)U(2k_3 + 1)U(2k_4 + 1) \right|^2 \end{aligned} \quad (43)$$

where the sum in the right-hand side is equal to $Y_{S,\text{odd}}(2m + 1)$. We replace $U(2l)$ in the left-hand side of (43) by (38), where $U(2l + 1)$ is replaced by $U(2l - 1)$, and take into account that

$$\sum_{k_1} \alpha U(2k_1 + 1)|U(2l - 1)| e^{j\angle U(2l)} \approx Y_{S,\text{even}}(2m).$$

Following the same lines of Section F1, we get

$$\text{var}(Y_{S,\text{even}}(2m)) \ll \frac{\mathbb{E}\{|U(2m + 1)|^2\}}{\mathbb{E}\{|U(2m)|^2\}} \text{var}(Y_{S,\text{odd}}(2m + 1)). \quad (44)$$

Combining (20) with (44) finally proves (22).

ACKNOWLEDGMENT

This work is an extended version of the conference proceeding paper [14].

REFERENCES

- [1] J. Schoukens, T. Dobrowiecki, and R. Pintelon, "Parametric identification of linear systems in the presence of nonlinear distortions," *IEEE Trans. Autom. Control*, vol. AC-43, no. 2, pp. 176–190, Feb. 1998.
- [2] J. Schoukens, R. Pintelon, and T. Dobrowiecki, "Linear modeling in the presence of nonlinear distortions," *IEEE Trans. Instrum. Meas.*, vol. 51, no. 4, pp. 786–792, Aug. 2002.
- [3] M. Enqvist and L. Ljung, "Linear approximations of nonlinear FIR systems for separable input processes," *Automatica*, vol. 41, no. 3, pp. 459–473, Mar. 2005.
- [4] M. Enqvist, "Linear models of nonlinear systems," Ph.D. dissertation, Dept. Elect. Eng., Linköping Univ., Linköping, Sweden, 2005.
- [5] P. M. Makila, "LTI approximation of nonlinear systems via signal distribution theory," *Automatica*, vol. 42, no. 6, pp. 917–928, Jun. 2006.
- [6] T. P. Dobrowiecki and J. Schoukens, "Linear approximation of weakly nonlinear MIMO systems," *IEEE Trans. Instrum. Meas.*, vol. 56, no. 3, pp. 887–894, Jun. 2007.
- [7] J. Schoukens, J. Lataire, R. Pintelon, G. Vandersteen, and T. Dobrowiecki, "Robustness issues of the equivalent linear representation of a nonlinear system," *IEEE Trans. Instrum. Meas.*, vol. 58, no. 5, pp. 1737–1745, May 2009.
- [8] C. Evans and D. Rees, "Nonlinear distortions and multisine signals—Part I: Measuring the best linear approximation," *IEEE Trans. Instrum. Meas.*, vol. 49, no. 3, pp. 602–609, Jun. 2000.
- [9] R. Pintelon, G. Vandersteen, L. De Locht, Y. Rolain, and J. Schoukens, "Experimental characterization of operational amplifiers: A system identification approach—Part I: Theory and simulations," *IEEE Trans. Instrum. Meas.*, vol. 53, no. 3, pp. 854–862, Jun. 2004.
- [10] R. Pintelon, Y. Rolain, G. Vandersteen, and J. Schoukens, "Experimental characterization of operational amplifiers: A system identification approach—Part II: Calibration and measurements," *IEEE Trans. Instrum. Meas.*, vol. 53, no. 3, pp. 863–876, Jun. 2004.
- [11] E. Wernholt and S. Gunnarsson, "Estimation of nonlinear effects in frequency domain identification of industrial robots," *IEEE Trans. Instrum. Meas.*, vol. 57, no. 4, pp. 856–863, Apr. 2008.
- [12] R. Pintelon and J. Schoukens, "Measurement and modeling of linear systems in the presence of non-linear distortions," *Mech. Syst. Signal Process.*, vol. 16, no. 5, pp. 785–801, Sep. 2002.
- [13] L. De Locht, G. Vandersteen, Y. Rolain, and R. Pintelon, "Estimating parameterized scalable models from the best linear approximation of nonlinear systems for accurate high-level simulations," *IEEE Trans. Instrum. Meas.*, vol. 55, no. 4, pp. 1186–1191, Aug. 2006.
- [14] R. Pintelon and J. Schoukens, "The best linear approximation of nonlinear systems operating in feedback," in *Proc. I2MTC*, Gratz, Austria, May 14–16, 2012, pp. 2092–2097.
- [15] P. E. Wellstead, "Reference signals for closed-loop identification," *Int. J. Control*, vol. 26, no. 6, pp. 945–962, 1977.
- [16] P. E. Wellstead, "Non-parametric methods of system identification," *Automatica*, vol. 17, no. 1, pp. 55–69, Jan. 1981.
- [17] R. Pintelon and J. Schoukens, *System Identification: A Frequency Domain Approach*, 2nd ed. Hoboken, NJ: Wiley-IEEE Press, 2012.
- [18] M. Schetzen, *The Volterra and Wiener Theories of Nonlinear Systems*. New York: Wiley, 1980.
- [19] D. R. Brillinger, *Time Series: Data Analysis and Theory*. New York: McGraw-Hill, 1981.
- [20] R. Pintelon and J. Schoukens, "Identification of continuous-time systems using arbitrary signals," *Automatica*, vol. 33, no. 5, pp. 991–994, May 1997.
- [21] R. Pintelon, J. Schoukens, and G. Vandersteen, "Frequency domain system identification using arbitrary signals," *IEEE Trans. Autom. Control*, vol. 42, no. 12, pp. 1717–1720, Dec. 1997.
- [22] R. Pintelon, K. Barbé, G. Vandersteen, and J. Schoukens, "Improved (non-)parametric identification of dynamic systems excited by periodic signals," *Mech. Syst. Signal Process.*, vol. 25, no. 7, pp. 2683–2704, Oct. 2011.
- [23] T. P. Dobrowiecki and J. Schoukens, "Measuring a linear approximation to weakly nonlinear MIMO systems," *Automatica*, vol. 43, no. 10, pp. 1737–1751, Oct. 2007.
- [24] E. Lukacs, *Stochastic Convergence*. New York: Academic Press, 1975.
- [25] R. Pintelon and J. Schoukens, "Measurement of frequency response functions using periodic excitations, corrupted by correlated input/output errors," *IEEE Trans. Instrum. Meas.*, vol. 50, no. 6, pp. 1753–1760, Dec. 2001.



Rik Pintelon (M'90–SM'96–F'98) was born in Gent, Belgium, on December 4, 1959. He received the M.S. degree in electrical engineering in 1982, the Ph.D. degree in engineering in 1988, and the qualification to teach at university level (geaggregeerde voor het hoger onderwijs) in 1994, all from the Vrije Universiteit Brussel (VUB), Brussels, Belgium.

From 1982 to 1984 and 1986 to 2000, he was a Researcher with the Belgian National Fund for Scientific Research (FWO-Vlaanderen) at the Electrical Engineering (ELEC) Department of the VUB. From 1984 to 1986, he did his military service overseas in Tunisia at the Institut National Agronomique de Tunis. From 1991 to 2000, he was a part-time Lecturer with the Department of ELEC of the VUB, and since 2000, he has been a Full-Time Professor in electrical engineering at the same department. His main research interests include system identification, signal processing, and measurement techniques. He is the coauthor of four books and about 200 articles in refereed international journals.

Dr. Pintelon is the recipient of the 2012 IEEE Joseph F. Keithley Award in Instrumentation and Measurement (IEEE Technical Field Award).



Johan Schoukens (M'90–SM'92–F'97) was born in Belgium in 1957. He received the M.S. degree in engineering and the Ph.D. degree in applied sciences from the Vrije Universiteit Brussel (VUB), Brussels, Belgium, in 1980 and 1985, respectively.

From 1981 to 2000, he was a Researcher with the Belgian National Fund for Scientific Research (FWO-Vlaanderen) at the Department of Electrical Engineering of the VUB, where he is currently a Full-Time Professor in electrical engineering. His main research interests include system identification, signal processing, and measurement techniques.

Dr. Schoukens was the recipient of the 2002 Andrew R. Chi Best Paper Award of the IEEE TRANSACTIONS ON INSTRUMENTATION AND MEASUREMENT, the 2002 Society Distinguished Service Award from the IEEE Instrumentation and Measurement Society, and the 2007 Belgian Francqui Chair at the Université Libre de Bruxelles, Brussels, Belgium. Since 2010, he has been a member of the Royal Flemish Academy of Belgium for Sciences and Arts. In 2011, he received a doctorate degree honoris causa from the Budapest University of Technology and Economics, Budapest, Hungary.